Froth properties and entrainment in lab-scale flotation: A case of carbonaceous sedimentary phosphate ore

Hoang, D. H.; Heitkam, S.; Kupka, N.; Hassanzadeh, A.; Peuker, U. A.; Rudolph, M.;

Froth properties and entrainment in lab-scale flotation: A case of carbonaceous sedimentary phosphate ore

Duong Huu Hoang[1, 2, 3, *], Sascha Heitkam[4], Nathalie Kupka[1], Ahmad Hassanzadeh[1], Urs A. Peuker[2], Martin Rudolph[1]

[1]*Department of Processing, Helmholtz Institute Freiberg for Resource Technology, Helmholtz-Zentrum Dresden-Rossendorf, Chemnitzer Straße 40, Freiberg, Germany*

[2]*Institute of Mechanical Process Engineering and Mineral Processing, Technische Universität Bergakademie Freiberg, Agricolastraße 1, Freiberg, Germany*

[3]*Department of Mineral Processing, Faculty of Mining, Hanoi University of Mining and Geology, Duc Thang, Bac Tu Liem, Hanoi, Vietnam*

[4]*Department of Transport Processes at Interfaces, Institute of Fluid Dynamics, Helmholtz-Zentrum Dresden-Rossendorf, Bautzner Landstraße 400, 01328 Dresden, Germany*

Corresponding author: d.hoang@hzdr.de / duongtvm@gmail.com   Tel: +49 351 260 4482

Graphical abstract: Flotation cell schematically represented as interacting pulp and froth zones in derivation of overall recovery and measuring the froth structure using DFA
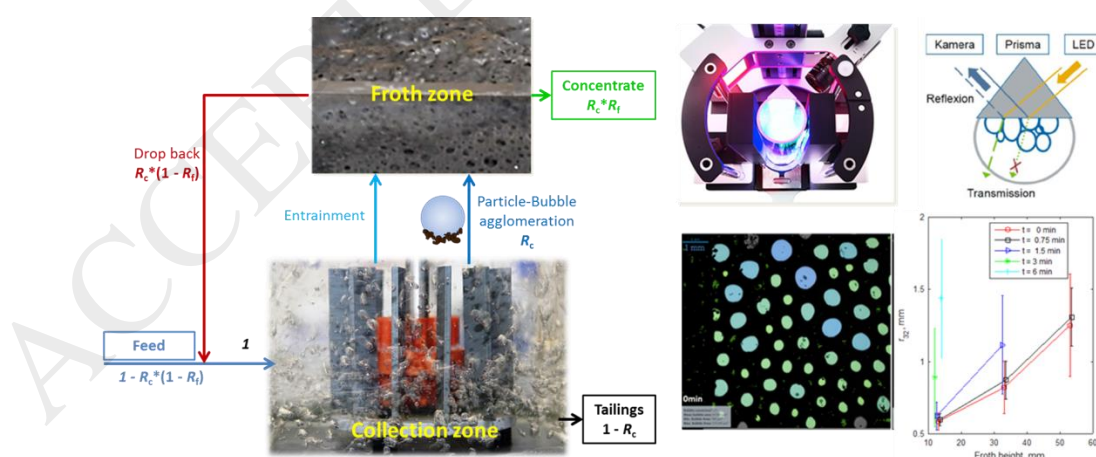
Highlights

- ❖ Batch flotation of high-grade ores are significantly changing froth properties
- ❖ The effects governing in the froth with time and allow relating to existing models
- ❖ The froth and pulp properties should be incorporated in the entrainment modeling
- ❖ The analyses offer novel support for the understanding of entrainment phenomena

Abstract

In flotation, the froth characteristics strongly influence the separation process as they are linked to water recovery, bubble size, entrainment of gangue particles, flotation rate constants and finally grade and recovery. In the case of a high-grade apatite ore with a high mass pull in lab-scale flotation, significant changes in pulp and froth properties occur, such that the froth stability decreases with increasing flotation time. These changes can be related to different particle and reagent concentrations. We describe the change of entrainment in a rich apatite ore batch flotation with time more precisely by measuring froth properties using a Dynamic Froth Analyzer (DFA). It is concluded that the degree of entrainment is not only dependent on particle size but also the pulp density due to its effect on particle settling and also froth properties in varying resistance to drainage. Through a combination of time-resolved dynamic froth analysis and automated mineralogy, we identify the dynamic effects governing in the froth and compare the entrainment results with existing models. Furthermore, our analyses offer novel support for the extension of the common understanding of the entrainment phenomena.

1. Introduction

Froth flotation belongs to the group of heterocoagulation separation techniques. It is classically divided into two active zones, the pulp zone, where particle collection occurs

and the froth zone, where the froth recovery of particles is governed by true flotation, drop back and entrainment.

In froth flotation, the collision probability in the collection zone is governed by the hydrodynamics of particle-bubble interactions (Wills and Finch, 2016). The true flotation event occurs when hydrophobic mineral particles collide with bubbles, attach in the liquid-gas interface and form stable particle-bubble aggregates lifted upwards against gravity towards the froth zone (Yianatos et al., 2009).

There are mechanical transportation processes of hydrophilic gangue minerals occurring within the froth phase including entrapment, entrainment, and recovery by composite particles and slime coatings. Unlike true flotation, entrainment is not chemically selective and is a mechanical mass transfer process by which particles suspended in the water between bubbles enter the flotation froth from the top pulp region and are transferred through the froth layer into the concentrate (Wang et al., 2015).

This study focusses on the characterization of the froth phase especially on the change of froth properties during lab-scale flotation of rich carbonaceous apatite ore. In addition, the entrainment modelling is discussed in detail and common models are applied to predict the degree of entrainment.

1.1. Froth phase characterization

Froth properties strongly influence final grade and recovery of valuable minerals in the concentrate launder, as well as control the amount of water recovered, and thus the amount of entrainment (Neethling and Brito-Parada, 2018). The primary role of the froth phase is to create an environment for the separation of valuable minerals attached to bubbles from gangue minerals in the slurry. It leads to transporting the precious materials from the bulk slurry to the concentrate launder (Heath, 2013). Although the importance of froth is widely acknowledged, there is considerable lack of studies concerning the characterization of froth properties due to its complex three-phase interfacial nature compromising air bubbles, solids and liquid, contrary to better studied foam systems that only comprise the liquid and gas phase. Solid particles can have a stabilising effect on the froth through an increase in the effective viscosity hindering the drainage of water within the bubble film as the solid particles are trapped within the Plateau border and ensuring increased roughness of the lamellae respectively (Marozva, 2015). In metal foam production particles inside the lamellas are even at the origin of the foam stability (Banhart, 2006).

Froth ability and stability: There is no standard coefficient of frothing; froths are characterized by their froth ability and their froth stability. The froth ability referred to as froth capacity, which is the quantitative assessment of the froth height or volume. This is usually measured at steady-state conditions. The static froth stability often relates to the lifetime of the froth (after the generation or bubbling step has been completed) (Farrokhpay, 2011; Pugh, 2016). Froth stability mainly depends on the typically non-ionic amphiphilic frothers (type and concentration) as well as the suspended particles, in particular with respect to particle hydrophobicity and size (Schwarz and Grano, 2005)

In flotation, the froth needs to be dynamically stable whilst bubbling is occurring, i.e. stable against bubble coalescence in the froth. However, it should be unstable without

bubbling further, i.e. in the launder, in order to results in a froth depleted suspension which can be further handled by pumping or filtration.

Froth structure: The froth structures elaborated on the pulp surfaces in froth flotation cells can provide useful information with respect to both grade and recovery of valuable minerals. Generally, digital image processing techniques are used for froth structure characterization in industrial flotation cells (Moolman et al., 1995).

Measurements of froth ability and stability:

There are several techniques which have been published in the literature to analyze froth properties such as X-ray microtomography (XµT) (Richardson et al., 2005; Stock, 1999, 2008), Dynamic Neutron Radiography (dNR) (Heitkam et al., 2018) and Magnetic resonance imaging (MRI) (Blümich, 1995, 2000; Laity et al., 2010; Richardson et al., 2005).

In this study, a Dynamic Froth Analyser (DFA) is used for evaluation of the froth ability/stability. Froth height and lifetime of a bubble are quantitative parameters representing the dynamic stability. In the DFA technique, the froth rises within a column and the height is measured as a function of time. The maximum froth height is defined as the froth reaches a horizontal asymptote, i.e. gas release rate of bursting bubble at the top of the froth is equal to the flow rate of gas into the suspension. The maximum height can be well correlated with the ability and stability of the froth (Pugh, 1996; Schwarz, 2004).

Several indicators have been introduced for assessment of the froth stability including froth half-life time, froth maximum height at equilibrium, bubble growth across the froth phase, air recovery and solid loading on bubbles on the top of the froth surface, froth velocity, and froth rise velocity (Farrokhpay, 2011). Bikerman (1973) determined the dynamic stability factor ($\sum$) as the ratio of the maximum volume of generated foam or froth to the gas flowrate given by Eq. 1. This factor has been used in froth flotation studies, e.g. Mackay et al. (2018), McFadzean et al. (2016a) and McFadzean et al. (2016b). There the effects of particle size on dynamic froth stability have been studied showing the link between dynamic froth stability and flotation performance.

$$\sum = \frac{V_f}{Q} = \frac{H_{max}A}{Q} \tag{Eq. 1}$$

where V_f is the froth volume, Q is the gas flowrate, H_{max} is the maximum equilibrium height and A is the cross-sectional area of the column.

The ratio physically translates to the average lifetime of bubbles in the froth. In addition to the maximum equilibrium height as a measure of froth stability, the froth rate has been applied (Marozva, 2015). Barbian et al. (2003) used the froth growth exponential model as a function of froth height and time:

$$H_f = H_{max}(1 - e^{-t/\tau}) \tag{Eq. 2}$$

where H_{max} and τ are the maximum equilibrium height and the average lifetime of bubbles in the froth phase, respectively.

1.2. Entrainment mechanisms and modelling

Entrainment is the main recovery mechanism for gangue minerals, especially the fine particles (Zheng et al., 2006). There are mainly three mechanisms, i.e. boundary layer, bubble wake, and bubble swarm effects, which account for the phenomena of mechanical

4

entrainment in froth flotation (Savassi et al., 1998; Smith and Warren, 1989; Wang et al., 2015).

Entrainment is mainly affected by the water recovery, pulp density, particle size, impeller speed (pulp density distribution), mineral specific gravity, particle hydrophobicity, superficial gas velocity, froth height, froth retention time, froth rheology and froth structure (Savassi et al., 1998; Wang et al., 2015).

The degree of entrainment (ENT_i) is defined as the ratio of the mass of mineral of size i per unit mass of water in the concentrate recovery by entrainment to the mass of mineral of size i per unit mass of water in the pulp (Johnson, 1972).

$$ENT_i = \frac{(\text{mass of free gangue particles per unit mass of water})_{\text{concentrate}}}{(\text{mass of free gangue particles per unit mass of water})_{\text{tailings}}}$$

In the pulp phase, a classification function i.e. CF_i is proposed to describe the state of solids suspension (Wang et al., 2015; Zheng et al., 2006), while in the froth phase the degree of entrainment (ENT_i) is proposed to describe the classification effect of the drainage of entrained particles (Bisshop, 1974; Kirjavainen, 1992; Savassi et al., 1998).

There are numerous, mostly empirical models aimed at describing mechanical entrainment of gangue particles into the concentrate. In this study, two common models of entrainment used in industry including Savassi and Yianatos models are applied to the experimental data of lab scale flotation test work.

The empirical partition curve proposed by Savassi et al. (1998) can be shown in Equation 3:

$$ENT_i = \frac{2}{\exp\left[2.292\left(\frac{d_{p,i}}{\xi}\right)^{\text{adj}}\right] + \exp\left[-2.292\left(\frac{d_{p,i}}{\xi}\right)^{\text{adj}}\right]} \qquad \text{(Eq. 3)}$$

$$adj = 1 - \frac{ln(1/\delta)}{exp(d_{p,i}/\xi)} \qquad \text{(Eq. 4)}$$

where ξ is the entrainment parameter defined as the particle size for which the degree of entrainment ENT_i equals 0.2, δ is the drainage parameter which is related to the degree of preferential entrainment of coarse particles. The entrainment parameter ξ is calculated based on the froth residence time of air which is given by: $\lambda_{air} = h_F/J_g$, where J_g is the superficial gas velocity ($J_g = V_g/A_{cell}$), h_F is the froth depth. The fitted values for the entrainment parameter ξ and the drainage parameter δ using the equation: $\xi = -0.667\lambda_{air} + 40.416$ and $\delta = 0.02\lambda_{air} + 0.534$, respectively.

Yianatos and Contreras (2010) proposed a particle entrainment model for industrial flotation cells using an entrainment factor EF_i as:

$$EF_i = \frac{R_{g,i}}{R_W} = exp\left[-0.693\left(\frac{d_{p,i}}{d_{p,0.5}}\right)^{\varphi}\right] \qquad \text{(Eq. 5)}$$

where $R_{g,i}$ is the gangue recovery of size class i, R_W is the water recovery, $d_{p,i}$ is the mean particle size of class i, $d_{p,0.5}$ corresponds to the mean particle size at $EF_i = 0.5$ for each data set (similar to d_{50} or cut size) ϕ is a drainage parameter depending on the mineral characteristics and cell operating conditions, that may be obtained by a least squares numerical method.

5

2. Material and methods

Ore: The carbonaceous sedimentary apatite ore used contains 64 % apatite, 27 % carbonates, 8 % various silicates (i.e. quartz, almandine, zircon, titanite, muscovite, sandine, albite, orthoclase, plagioclase and phlogopite) and 1 % other minerals. The ore is ground dry using a ball mill to reach a d_{80} of 50 µm. Figure 1 exhibits a schematic view of the preparation of the samples, conditioning and conducting the flotation experiments.

Froth flotation procedure and sample preparation for dynamic froth analysis with DFA-100: The batch flotation tests were performed using a mechanical cell built at the TU Bergakademie Freiberg, Germany. The detailed flotation procedures are described elsewhere (Hoang et al., 2018a; Hoang et al., 2017, 2018b). The flotation tests in this study were conducted with the impeller tip speed of 2.5 m/s using the double finger impeller type at an air flow rate of 2 l/min and solids content 8 vol. %, the reagents regime is shown in Figure 1.

The pulp in the flotation cell at the given flotation times (remaining pulp suspension) is collected right after the flotation tests. A 60 ml sample of this pulp is transferred to a transparent glass column of 40 mm inner diameter of the Dynamic Froth Analyzer DFA-100 (Krüss, Germany). As reported in Geldenhuys and McFadzean (2018) the diameter does have an effect on the dynamic froth stability, but since it is constant for all tested suspensions the results should be comparable amongst one another. Subsequently, the froth is generated by bubbling the air through a ceramic frit (pore diameter 16 µm – 45 µm) at 0.5 l/min air flow rate (standard conditions) for a constant duration of 100 s. The froth properties including its height and structure are recorded to evaluate dynamic parameters of the froth ability, froth stability and time-dependent bubble size distribution. The bubble size distribution is observed as well at different camera positions, i.e. froth heights, employing an adapted image processing algorithm described in section 3.3 below. The liquid content is derived from the electric conductivity, measured at up to seven height increments of the froth. Details of the measurement principle are given by Oetjen et al. (2014).

Reagents: Sodium hydroxide (NaOH) is provided by Carl Roth GmbH & Co. KG, Germany. Sodium carbonate (Na_2CO_3) 99.9 % from VWR Company, Belgium was applied as a pH modifier to achieve an alkaline environment. Sodium silicate (Na_2SiO_3), with a purity of 99 %, is supplied by Zschimmer & Schwarz GmbH & Co. KG, Germany. Corn starch (($C_6H_{10}O_5)_n$) is supplied by Carl Roth. It is gelatinized with NaOH at a 4:1 ratio Starch/NaOH and is used as carbonate depressant. Methyl isobutyl carbinol (MIBC) is used as a frother, provided by Sigma-Aldrich, Germany. The collector was Berol 2015, which is a formulation of an amphoteric collector and a non-ionic secondary collector supplied by AkzoNobel Surface Chemistry, Sweden.

Mineral Liberation Analysis: A detailed description of the sample preparation process for automated mineralogy with the Mineral Liberation Analyzer (MLA) can be found in previous studies Hoang et al. (2017, 2018b), Leißner et al. (2016a) and Leißner et al. (2016b). Twenty-four samples of all size-by-size sub-samples for the feed, concentrates and tailings are analysed with this automated mineralogical technique. The effect of particle size of hydrophilic minerals on the degree of entrainment is assessed at different flotation times. The ENT_i is calculated using the recovery of fully liberated assumingly hydrophilic silicates (100% of the free surface in each particle cross-section). Depending

6

on the particle size, between 303,000 to 670,000 liberated silicate particles in each size fraction obtained by MLA were included in the calculations for a sound statistical treatment of the individual particle information.

3. Results and Discussion

The lab-scale batch flotation of high-grade apatite ore leads to significant changes of pulp properties (Figure 11 and Figure 12a) and froth properties (froth structure and froth stability) with time. These changes are caused by the high mass pull which goes along with decreasing reagent and particle concentrations during the lab-scale flotation. This is an effect, which, to the best of our knowledge, has not been thoroughly addressed before.

3.1. Surface activity

The supernatants of the concentrates and pulps are characterized for their dynamic surface tension, i.e. surface tension at various ages of the surface after being created, using a bubble pressure tensiometer BP-100 (Krüss, Germany). Figure 3 demonstrates the dynamic surface tension term versus the surface age and its change as a function of the flotation time. It can be evidently seen that a decrease in surfactant concentrations with flotation time leads to an increase in the surface tension of the remaining pulp. The non-ionic frothers as well as the non-surface-bound amphoteric collectors appear to be highly surface active reducing the surface tension of the supernatants to less than 50 mN/m (Figure 2a). It is also significantly noticeable that the surface activity of the supernatants of the concentrates is substantially greater than those of the pulp (Figure 2b). Indeed, this emphasizes the enrichment of surface active frothers and free collectors in the concentrates, hence the term "frothing out". There is a faster adsorption of the surface active molecules into the liquid-gas interface of the supernatants of the concentrates (visible in the dashed curves in Figure 2a) as compared to the curves for the pulp supernatants. This could be due to a preferential enrichment of the small MIBC molecules which should have a higher diffusivity and a faster kinetics of adsorption as compared to the larger amphoteric collectors.

3.2. Froth ability and froth stability

A low dynamic surface tension usually should correspond to higher froth ability. However, the froth stability is more dependent on the viscoelasticity and repulsive interactions within thin film lamellae (Pugh, 2016). It is observed that as the flotation time increases (from P0 to P4) the froth height decreases (Figure 3a). It is attributed to the decrease in frothing reagent concentrations in the pulp due to the high mass pull. These results indicate that in the case of lab-scale flotation of rich apatite ore, froth ability and froth stability are significantly changing with flotation time.

The temporal froth height development before reaching the maximum can be fitted with an exponential function (Barbian et al., 2005; 2003) as shown in Figure 3b. The regression analysis gives values of the parameters τ and H_{max} corresponding to the characteristic average bubble lifetime and maximum height, respectively, which can be used as proxies

for froth stability. The rate of decreasing froth height after stopping of bubbling (at 100 s) is corresponding to the bubble burst rate.

The average lifetime of bubbles and the dynamic stability factor were both at 0.29 min before flotation. After 6 min flotation time, these values reduced to 0.03 min and 0.04 min, respectively.

As demonstrated in Figure 5a, the liquid content decreases from the base to the top of the froth through drainage. This is in line with the prediction by the foam drainage equation (Weaire et al., 1997). In order to reach a steady state, further down in the froth the cumulative water flow from above has to pass, which requires a higher drainage permeability and thus, higher liquid fraction. Additionally, coarsening takes place (see section 3.3 below) which results in larger bubbles in the upper part of the froth, yielding higher drainage permeability at a given liquid fraction and consequently, smaller liquid content.

In addition, Figure 5b, c, and d show the liquid content (degree of wetness) decreasing with increasing the flotation time at various fixed froth heights. This effect of reduced liquid content with flotation time is due to the significant reduction in both surfactant and particle concentrations. Firstly, the particle content directly hinders drainage along the plateau borders and thus, lower particle concentration results in higher drainage rate and consequently, less liquid content. Secondly, a lower surfactant concentration results in stronger coarsening of the froth (see section 3.3 below) and larger bubbles result in higher drainage permeability for a given liquid fraction (Cantat et al., 2013). Consequently, the foam dries faster.

3.3. Bubble size distribution

The bubble size is assessed by grey scale images from the plan-parallel side of the column. Due to total reflection, the thin lamellas between bubbles and wall appear bright while plateau borders appear dark. The particles suspended inside the lamellas withhold a bit of water around them, appearing also black and disturbing image processing. As seen in Figure 7, the bubble sizes in the froth phase are significantly increased with increasing flotation time. They become larger due to a reduction of the reagent concentrations and a decrease in the solids content in the pulp.

The images are treated similarly to the method proposed by Boos et al. (2013). Firstly, gaussian filtering with a radius of 20 pixels is employed in order to smoothen distortions from the particles positioned inside the lamellas (Figure 7b). Subsequently, binarization (Figure 7c) and a skeleton transformation (Figure 7d) virtually removes the thick, wall-touching Plateau borders and reveals the contact lines of the lamellas at the wall separating the bubbles. Each area bound by a set of contact lines represents the contact area of one bubble with the wall. Segmentation (Figure 7d) yields the size of all contact areas in the field of view. Objects close to the rim of the image or with an area smaller than 10 px^2 are ignored. The blue circles in Figure 7d mark all accepted bubble contact areas.

In this study, the bubble size is represented by the equivalent spherical radius r of the bubble volume and the contact area size is denoted by its equivalent circular radius r_s. Using the Surface Evolver, Wang and Neethling (2009) found the statistics for the relation of r and r_s:

$$f\left(\frac{r_s}{r}\right) = \frac{3.51(r_s/r)^{4.61}}{1 + exp\big(47.96(r_s/r - 1.08)\big)}$$

Employing the reconstruction algorithm of Wang and Neethling (2009), the corresponding distribution of the volume equivalent bubble radius r of the wall-touching bubbles is reconstructed. Taking into account all bubbles from all images for a certain flotation time and a certain foam height reveals the bubble size distributions presented in Figure 8a. From these distributions, the Sauter mean radius r_{32} is derived, presented in Figure 8b.

In Figure 8 it can be clearly seen that bubbles increase in size with froth height in the column. In general, two mechanisms for foam coarsening exist, i.e. gas diffusion and lamella rupture. Since the liquid content of the froth is high and the bubbles are relatively large, gas diffusion acts in the order of tens of minutes (Cantat et al., 2013) and hence, can be neglected. Consequently, the coarsening must be dominated by film rupture, which could result from the low concentration of surfactants as well as from the presence of hydrophobic particles suspended in the lamellas (Pugh, 1996).

This finding is in line with the reduced bubble lifetime in section 3.2. Reduction of the foam height and coarsening both results from lamella rupture.

In the literature, several models for the bubble size evolution in coarsening froth are developed (Park, 2015). However, employing these models requires well defined particle sizes, contact angles and concentration, which is not applicable to realistic ore samples such as in the present experiment. Developing a suitable froth coarsening model for realistic ore samples is beyond the scope of this paper, especially since the variations of r_{32} in Figure 8b is large, pointing toward a highly stochastic behaviour.

3.4. Water recovery, silicates recovery and degree of entrainment

The fully liberated silicate minerals identified in automated mineralogy are assumed as hydrophilic and they do not contain Ca^{2+} and Mg^{2+} ions which might lead to true flotation by surface activation. Consequently, these particles are recovered into the concentrate by entrainment only. Thus they are used as "natural tracer particles" to study entrainment effects.

9

3.4.1. Water recovery versus silicates recovery

Entrainment is strongly dependent on the water, which is the carrying medium to transfer the entrained mineral particles into the concentrate in flotation processes. In general, the correlation between the recovery by entrainment and the water recovery shows a linear trend for fine particles and a parabolic trend for coarse particles (Figure 9), which agrees with observations in (Wang et al., 2015; Zheng et al., 2006). Fine silicate particles are recovered by entrainment at a rate similar to the amount of water recovered while coarser hydrophilic particles drain more quickly from the froth to the pulp, i.e. against the upward movement of bubbles, and therefore are entrained into the concentrate at a lower rate than finer particles.

As expected, Figure 9 shows a clear correlation between the amount of cumulative water and fully liberated silicate particles recoveries. From these results, it can be concluded that it is important to control the froth zone to achieve a lower ratio between the water and mass recovery, i.e. a drier froth. This will lead to an increased grade of the concentrates.

3.4.2. Degree of entrainment

In the lab-scale flotation cell, the silicates concentration in the pulp decreases with flotation time as solid particles and water are continually removed during flotation, and additional water is added to maintain a constant pulp-level. In this study, the degree of entrainment for different flotation times is calculated based on the cumulative recovery of fully liberated silicates and the tailings concentration is that in the cell at the completion of the test.

Figure 10 shows the change of ENT_i and the average size of the manually sieved fractions of the fully liberated silicate particles as a function of flotation time (affecting pulp rheology and froth properties), which is only possible through automated mineralogical analysis. As can be seen in Figure 10, the mean size of liberated silicates particles is smaller than the manually sieved fractions.

For the finest fraction (0-20 μm), the ENT_i is slightly increasing with increasing flotation time. The average particle size in this fine fraction is almost constant with respect to the flotation time due to the low inertia of the particles and thus no settling related enrichment. In the pulp phase, fine particles are easily suspended in the water or the water film surrounding the bubbles in the region below the pulp/froth interface as compared to coarser particles and hence they have a higher chance to travel up through the froth into the concentrate (Wang et al., 2015).

For the intermediate and coarse fractions, the ENT_i and the silicate particle size are reduced with increasing flotation time. This variation is caused by the high mass pull of this lab-scale batch flotation of high-grade apatite ore leading to severe changes of pulp properties (particularly the pulp density), change in particle size and also froth properties (Hoang et al., 2017). The decrease of the pulp density and the froth stability with flotation time leads to an increase of the settling velocities and more likely drop back (drainage) to the pulp for coarser particles. This is an effect that has not been observed and mentioned before, to the best of our knowledge.

3.5. Modelling of entrainment

Figure 11 displays a reasonable agreement between the obtained experimental data at different flotation times and predicted results of both empirical models used. The model of Savassi (Savassi et al., 1998) fits well to intermediate sizes. The deviation for ultrafine particles may be caused by neglectance of mechanisms such as entrapment in the froth phase (Zheng et al., 2006). Yianatos' model shows a good fit for fine and coarse particles. However, in this study, the range of particle sizes is quite narrow and rather fine for all fractions studied (fine flotation at d_{80} of 50 µm). The ENT_i can be also described as a power function of the mean particle size with high R-squared. It can be found that the best fit function depends on the flotation time (pulp and froth properties), this might be influenced by other mechanisms such as entrapment in addition to entrainment in the water (Zheng et al., 2006). The models do not consider other important factors, i.e. cell operating conditions, pulp density, and drainage parameter.

The fitted values in Yianatos' model of the drainage parameter ϕ for different flotation times are shown in Figure 12a. An increase in the flotation time (decrease in pulp density) results in a decrease in its degree of entrainment that changes the drainage parameter in the model. Hence, in the lab-scale batch flotation of high-grade ores, the drainage parameters significantly dependent on flotation time due to a strong reduction of pulp density. This result must be taken into consideration for the development of entrainment models in batch conditions. In this regard, a number of studies also reported that there was an increase in the recovery of non-floatable gangue by increasing pulp density while water recovery was constant (Cilek, 2009; Warren, 1985) which is in good agreement with the presented outcomes. However, none of these studies proposed the simultaneous effect of pulp density and flotation time on the entrainment phenomenon.

As mentioned above and shown in Figure 11, the ENT can be also described as a power function of the mean particle size:

$$ENT = A * d_p{}^B \qquad\qquad (Eq.\ 6)$$

where A and B are constants which depend on the ore characteristics, froth properties, the cell design and operating conditions, and especially in this case the pulp density. The data shows a good correlation between values A and B over flotation time and pulp densities (cf. Figure 12a).

3.6. The effect of pulp density and particle settling velocity on the entrainment

As mentioned earlier, the change of pulp density is significant in this study due to a high mass pull. Differences in the ENT_i with different size and pulp densities are likely to be a consequence of differences in settling rate within the pulp, at the interface or froth phase where flow can be considered in the Stokes regime (Wang, 2017). Under these

conditions, the particle settling rate of entrained particles in the fluid can be approximated using Stokes' law (Smith and Warren, 1989).

Figure 12b illustrates a schematic diagram of hydraulic entrainment (boundary layer) as the most common mechanism of transporting the valuable and gangue minerals to the froth zone. As seen, the precious materials (apatite) along with unwanted minerals (carbonates and silicates) trap between the bubbles and entrain to the concentrate

The amount of water flowing upward and downward is changing by variation of the flotation time and the froth height. There is a great variation in liquid holdup from the pulp/froth interface to the froth surface, liquid velocity varies with position due to a change in water content in the froth (Neethling and Cilliers, 2009). Liquid holdup decreases with height in the froth due to drainage. An increase in the liquid velocity as it rises within the froth and therefore the drag force increases upon the particles.

(Neethling and Cilliers, 2002a, b) proposed that the motion of the entrained materials in the froth is a consequence of a balance between liquid motion, particle settling and particle dispersion. The amount of material entrained to the concentrate is determined by the net flow of water including suspended solid particles upwards (Wang, 2017). There are three distinct regions within the froth zone. Region 1 is just above the pulp/froth interface where there is a rapid decrease in gangue solid concentration due to rapid decrease in water content. Region 2 is in the center of the froth layer, where the balance of the liquid motion and the hindered solid settling determines the relative motion of the gangue particles, resulting in a steady reduction in the concentration of gangue particles as the height from the pulp/froth interface increases. In the upper region 3, the gangue particle concentration remains relatively constant, due to there being no relative downward motion of the solids with respect to the water in this region.

The motion of solid particles at the interface may depend on the settling and drag forces acting upon the particles. According to the Bubble Swarm Theory, the interface region is where water and suspended solid particles are being pushed upwards by rising air bubbles (Wang, 2017).

Steinour (1944) studied the sedimentation of small uniform particles, using the viscosity of the fluid, the density of the suspension and a function of the voidage of the suspension to take account of the character of the flow spaces. The apparent settling velocity of particles within the froth undergoing hindered settling under laminar conditions can be estimated from the following (Ray, 1993; Richardson and Zaki, 1997):

$$v_{\text{settling},i} = \frac{(\rho_s - \rho_f)g d_{i2}}{18\mu_i} e^2 \, 10^{-1.82(1-e)} \qquad \text{(Eq. 7)}$$

where, ρ_s and ρ_f are the densities of silicates particle (2,650 kg/m^3) and water (1,000 kg/m^3), respectively and g is the gravitational acceleration (9.81 m/s^2), ε is the voidage of suspension, μ_i is the viscosity of pulp; it can be calculated approximately from the volume fraction and the viscosity of the liquid using Einstein's equation:

$$\mu_i = \mu_w(1 + 2.5\varphi_{pulp,i}) \qquad\qquad (Eq.\ 8)$$

where μ_w is the dynamic viscosity of water (1.002 mPa·s) and $\phi_{pulp,i}$ is volume fraction at flotation time i.

Figure 12c shows the degree of entrainment plotted against $v_{settling}$ and mean fully liberated silicates size of different fractions at different flotation times. As can be seen, the degree of entrainment is correlating with $v_{settling}$ over flotation time, suggesting that the particle settling rate is the key factor (Wang, 2017).

A power relationship was observed between the ENT and a function related to the particle settling rate and pulp viscosity (Figure 12c). The particle settling velocity increases with the increasing particle size due to an increase in the apparent immersed weight of the coarser particles.

4. Conclusions

We investigated the froth properties (froth ability, stability, and its structure) in a lab-scale batch flotation process of a high grade carbonaceous sedimentary phosphate ore. The experiments were conducted under different flotation time values (0, 0.75, 1.5, 3 and 6 min). Additionally, the degree of entrainment together with its modelling was studied using the two most common models (i.e. Savassi and Yianatos). The effect of pulp density and particle settling velocity on the entrainment was evaluated using Richardson and Zaki's approach. The froth characteristics were quantitatively measured using the dynamic froth analysis (DFA) technique. The liberation degrees of the silicate minerals were identified by means of automated mineralogy (MLA). The degree of entrainment was calculated based on purely hydrophilic particles in automated mineralogy data and the surface activity of reagents was characterized with bubble pressure tensiometry.

This work contributes to the common understanding as follows:

- we have highlighted the significantly changing pulp and froth properties with time when processing high-grade ores in lab scale batch flotation test work which is also relevant along with a rougher bank in continuous flotation;

- through a combination of time-resolved dynamic froth analysis and automated mineralogy we have identified the effects governing in the froth with different flotation times and compared the entrainment results with existing models;
- our analyses offer novel support for the common understanding of the phenomena of entrained suspended particles within froth lamella.

It was revealed that the froth structure and froth stability (i.e. froth height, bubble size and liquid content) were significantly altered with respect to decreasing reagent and particle concentrations during the lab-scale flotation tests. The results show a decreasing entrainment with time for coarse particles due to changing sedimentation of those hydrophilic silicate particles, increased froth drainage and decreasing stability of the bubble films in the froth layer. Furthermore, the size of fully liberated silicate particles in the fine fraction was almost constant, while the size of coarser fractions decreased with flotation time. This effect was only possible to observe through consequent application of automated mineralogy and, to our best of knowledge, has not been reported before.

Both models of Savassi and Yianatos showed a very good fit to the experimental data for fully liberated silicates. The obtained results showed that not only particle size and density but specifically also the froth and pulp properties should be incorporated in future entrainment models. The effect of particle size and pulp density on the degree of entrainment might be caused by both factors affecting the sedimentation velocity of gangue particles which has also been identified as an important component in the fundamental model of Neethling and Cilliers (2009).

References

Banhart, J., 2006. Metal Foams: Production and Stability. Advanced Engineering Materials 8, 781-794.

Barbian, N., Hadler, K., Ventura-Medina, E., Cilliers, J.J., 2005. The froth stability column: linking froth stability and flotation performance. Minerals Engineering 18, 317-324.

Barbian, N., Ventura-Medina, E., Cilliers, J.J., 2003. Dynamic froth stability in froth flotation. Minerals Engineering 16, 1111-1116.

Bikerman, J.J., 1973. Foams. Springer-Verlag, New York.

Bisshop, J.P., 1974. A Study of Particle Entrainment in Flotation Froths. University of Queensland.

Blümich, B., 1995. P. T. Callaghan. Principles of nuclear magnetic resonance microscopy. Oxford University Press, Oxford, 1993, 492 pp, £25. ISBN 0 198 53997 5. Magnetic Resonance in Chemistry 33, 322-322.

Blümich, B., 2000. NMR imaging of materials. OUP Oxford.

Boos, J., Drenckhan, W., Stubenrauch, C., 2013. Protocol for Studying Aqueous Foams Stabilized by Surfactant Mixtures. Journal of Surfactants and Detergents 16, 1-12.

Cantat, I., Cohen-Addad, S., Elias, F., Graner, F., Höhler, R., Pitois, O., Rouyer, F., Saint-Jalmes, A., Cox, S., 2013. Foams: Structure and Dynamics. 102-110.

Cilek, E.C., 2009. The effect of hydrodynamic conditions on true flotation and entrainment in flotation of a complex sulphide ore. International Journal of Mineral Processing 90, 35-44.

Farrokhpay, S., 2011. The significance of froth stability in mineral flotation-a review. Advances in colloid and interface science 166, 1-7.

Geldenhuys, S., McFadzean, B., 2018. Column diameter effects on dynamic froth stability measurement, International Mineral Processing Congress XXIX, Moscow, Russia.

Heath, J., 2013. Frothing at the lip - stability in your flotation cell - Outotec.

Heitkam, S., Rudolph, M., Lappan, T., Sarma, M., Eckert, S., Trtik, P., Lehmann, E., Vontobel, P., Eckert, K., 2018. Neutron imaging of froth structure and particle motion. Minerals Engineering 119, 126-129.

Hoang, D.H., Kupka, K., Peuker, U.A., Rudolph, M., 2018a. Froth properties and its effect on lab-scale flotation of a carbonaceous sedimentary apatite ore, International Mineral Processing Congress XXIX, Moscow, Russia.

Hoang, D.H., Kupka, N., Peuker, U.A., Rudolph, M., 2017. Flotation study of a fine grained carbonaceous sedimentary apatite ore – challenges in process mineralogy and impact of hydrodynamics, Flotation' 17, Cape Town, South Africa.

Hoang, D.H., Kupka, N., Peuker, U.A., Rudolph, M., 2018b. Flotation study of fine grained carbonaceous sedimentary apatite ore – Challenges in process mineralogy and impact of hydrodynamics. Minerals Engineering 121, 196-204.

Johnson, N.W., 1972. The flotation behaviour of some chalcopyrite ores. University of Queensland Press, St. Lucia, Queensland.

Kirjavainen, V.M., 1992. Mathematical model for the entrainment of hydrophilic particles in froth flotation. International Journal of Mineral Processing 35, 1-11.

Laity, P.R., Mantle, M.D., Gladden, L.F., Cameron, R.E., 2010. Magnetic resonance imaging and X-ray microtomography studies of a gel-forming tablet formulation. European Journal of Pharmaceutics and Biopharmaceutics 74, 109-119.

Leißner, T., Duong, H.H., Rudolph, M., Heinig, T., Bachmann, K., Gutzmer, J., Schubert, H., Peuker, U.A., 2016a. Investigation of mineral liberation by transgranular and intergranular fracture after milling, IMPC 2016 - 28th International Mineral Processing Congress.

Leißner, T., Hoang, D.H., Rudolph, M., Heinig, T., Bachmann, K., Gutzmer, J., Schubert, H., Peuker, U.A., 2016b. A mineral liberation study of grain boundary fracture based on measurements of the surface exposure after milling. International Journal of Mineral Processing 156, 3-13.

Mackay, I., Mendez, E., Molina, I., Videla, A.R., Cilliers, J.J., Brito-Parada, P.R., 2018. Dynamic froth stability of copper flotation tailings. Minerals Engineering 124, 103-107.

Marozva, T., 2015. Investigating the effect of frother type on froth stability, froth recovery and entrainment, Department of Chemical Engineering. University of Cape Town.

McFadzean, B., Achaye, I., Chidzanira, T., Harris, M., 2016a. The effect of particle size on froth stabilities of different ores, XXVIII International Mineral Processing Congress Proceedings, Quebec, Canada.

McFadzean, B., Marozva, T., Wiese, J., 2016b. Flotation frother mixtures: Decoupling the sub-processes of froth stability, froth recovery and entrainment. Minerals Engineering 85, 72-79.

Moolman, D.W., Aldrich, C., van Deventer, J.S.J., Stange, W.W., 1995. The classification of froth structures in a copper flotation plant by means of a neural net. International Journal of Mineral Processing 43, 193-208.

Neethling, S.J., Brito-Parada, P.R., 2018. Predicting flotation behaviour – The interaction between froth stability and performance. Minerals Engineering 120, 60-65.

Neethling, S.J., Cilliers, J.J., 2002a. The entrainment of gangue into a flotation froth. International Journal of Mineral Processing 64, 123-134.

Neethling, S.J., Cilliers, J.J., 2002b. Solids motion in flowing froths. Chemical Engineering Science 57, 607-615.

Neethling, S.J., Cilliers, J.J., 2009. The entrainment factor in froth flotation: Model for particle size and other operating parameter effects. International Journal of Mineral Processing 93, 141-148.

Oetjen, K., Bilke-Krause, C., Madani, M., Willers, T., 2014. Temperature effect on foamability, foam stability, and foam structure of milk. Colloids and Surfaces A: Physicochemical and Engineering Aspects 460, 280-285.

Park, S., 2015. Modeling Bubble Coarsening in Froth Phase from First Principles, Blacksburg, Virginia.

Pugh, R.J., 1996. Foaming, foam films, antifoaming and defoaming. Advances in colloid and interface science 64, 67-142.

Pugh, R.J., 2016. Bubble and Foam Chemistry. Cambridge University Press.

Ray, M.S., 1993. Chemical Engineering, Volume 2: Particle Technology and Separation Processes, 4th edn, by J.M. Coulson and J.F. Richardson. Pergamon Press, Oxford, UK. 1991. 968 pp. ISBN 0-08-037957-5. Developments in Chemical Engineering and Mineral Processing 1, 172-172.

Richardson, J.C., Bowtell, R.W., Mäder, K., Melia, C.D., 2005. Pharmaceutical applications of magnetic resonance imaging (MRI). Advanced Drug Delivery Reviews 57, 1191-1209.

Richardson, J.F., Zaki, W.N., 1997. Sedimentation and fluidisation: Part I. Chemical Engineering Research and Design 75, S82-S100.

Ross, V.E., Van Deventer, J.S.J., 1988. Mass transport in flotation column froths, Column Flotation'88, Phoenix, Arizona, pp. 129–139.

Savassi, O.N., Alexander, D.J., Franzidis, J.P., Manlapig, E.V., 1998. An empirical model for entrainment in industrial flotation plants. Minerals Engineering 11, 243-256.

Schwarz, S., 2004. The relationship between froth recovery and froth structure, Ian Wark Research Institute. University of South Australia.

Schwarz, S., Grano, S., 2005. Effect of particle hydrophobicity on particle and water transport across a flotation froth. Colloids and Surfaces A: Physicochemical and Engineering Aspects 256, 157-164.

Smith, P.G., Warren, L.J., 1989. Entrainment of Particles into Flotation Froths. Mineral Processing and Extractive Metallurgy Review 5, 123-145.

Steinour, H.H., 1944. Rate of sedimentation.Nonflocculated Suspensions of Uniform Spheres. Industrial & Engineering Chemistry 36, 618-624.

Stock, S.R., 1999. X-ray microtomography of materials. International Materials Reviews 44, 141-164.

Stock, S.R., 2008. Recent advances in X-ray microtomography applied to materials. International Materials Reviews 53, 129-181.

Wang, L., 2017. Entrainment of fine particles in froth flotation. The University of Queensland.

Wang, L., Peng, Y., Runge, K., Bradshaw, D., 2015. A review of entrainment: Mechanisms, contributing factors and modelling in flotation. Minerals Engineering 70, 77-91.

Wang, Y., Neethling, S.J., 2009. The relationship between the surface and internal structure of dry foam. Colloids and Surfaces A: Physicochemical and Engineering Aspects 339, 73-81.

Warren, L.J., 1985. Determination of the contributions of true flotation and entrainment in batch flotation tests. International Journal of Mineral Processing 14, 33-44.

Weaire, D., Hutzler, S., Verbist, G., Peters, E., 1997. A Review of Foam Drainage. In Advances in Chemical Physics 102.

Wills, B.A., Finch, J.A., 2016. Chapter 12 - Froth Flotation, Wills' Mineral Processing Technology (Eighth Edition). Butterworth-Heinemann, Boston, pp. 265-380.

Yianatos, J., Contreras, F., 2010. Particle entrainment model for industrial flotation cells. Powder Technology 197, 260-267.

Yianatos, J., Contreras, F., Díaz, F., Villanueva, A., 2009. Direct measurement of entrainment in large flotation cells. Powder Technology 189, 42-47.

Zheng, X., Johnson, N.W., Franzidis, J.P., 2006. Modelling of entrainment in industrial flotation cells: Water recovery and degree of entrainment. Minerals Engineering 19, 1191-1203.
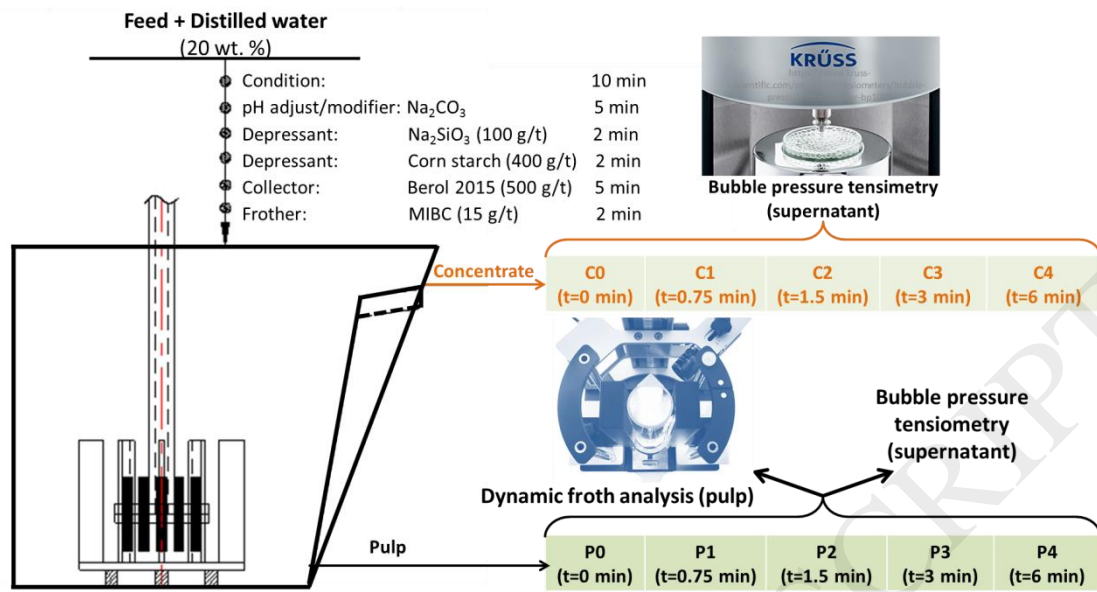
Figures

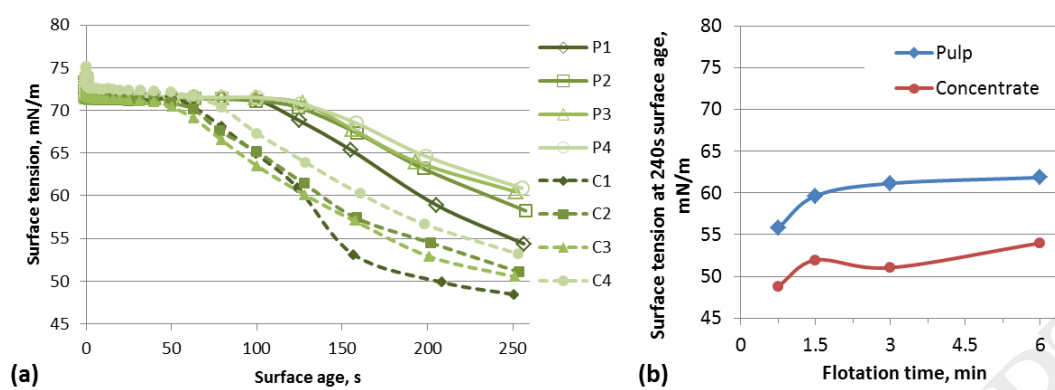*Figure 1- A scheme of flotation and sample preparation procedures*

Figure 2 - a) Dynamic surface tension as a function of surface age of the pulp and concentrates after various flotation times b) The change of surface tension at 240 s surface age of pulps and concentrates with flotation time
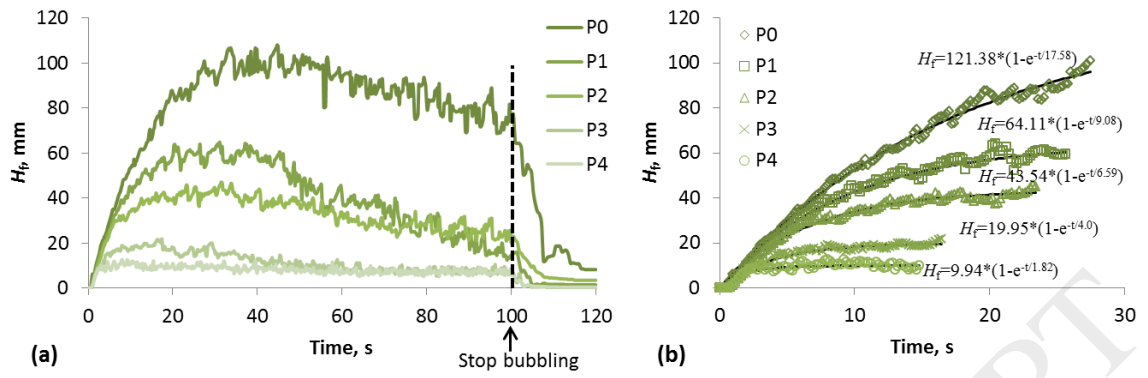
*Figure 3 - Froth height as a function of measuring time during growth of froth of pulp samples at various flotation times (**a**) and the froth growth exponential models (**b**)*
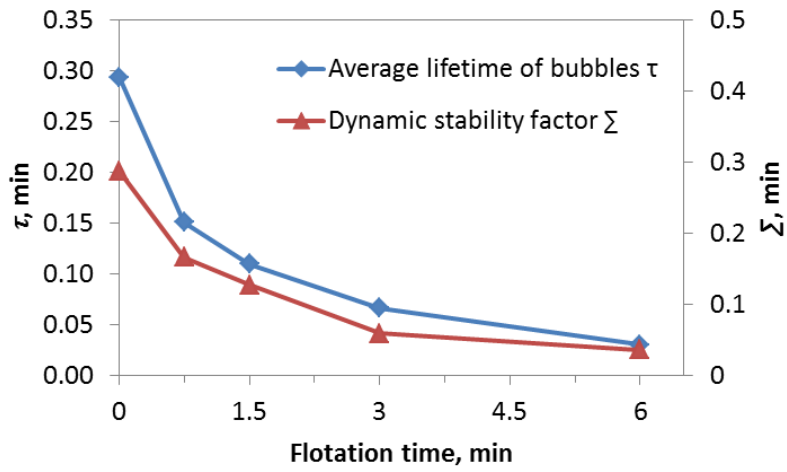
Figure 4- Average lifetime of bubble τ and dynamic stability factor ∑ as a function of flotation time (τ and Hmax from Figure 3b, A= 1256.64 mm² and Q = 0.5 l/min)
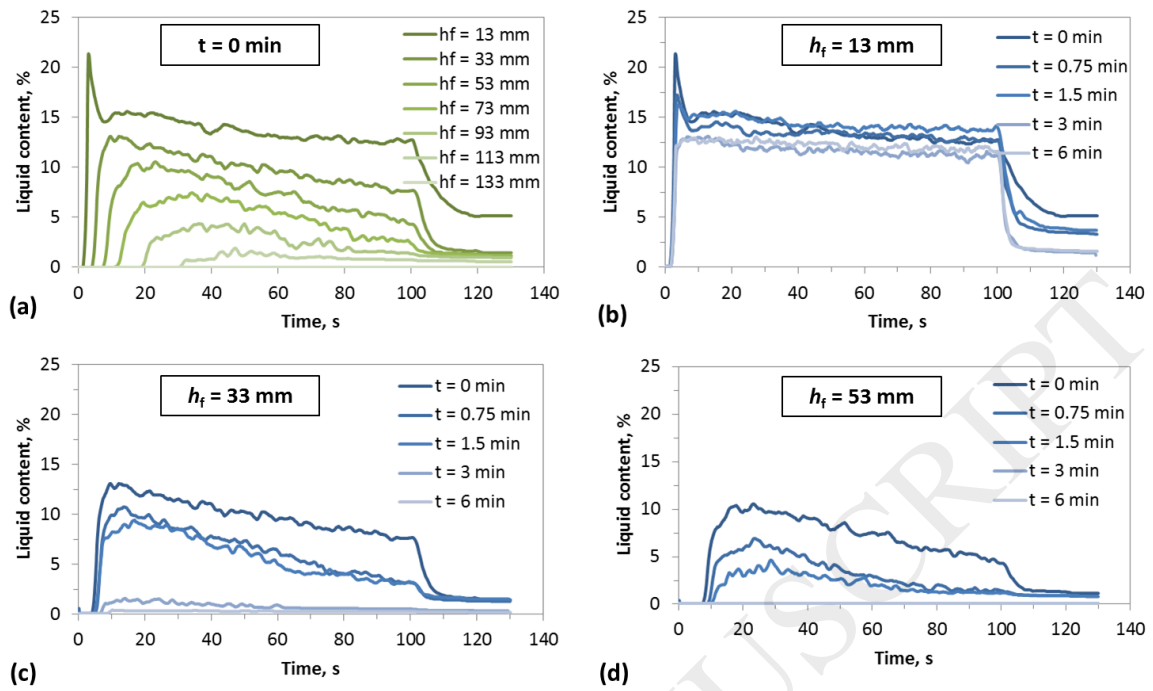
Figure 5 – a) The change of liquid content for the seven sensors of the conductivity electrode (h_f=13 mm to 133 mm) from the bottom to the top of pulp sample after 0 min flotation time and time dependence of the liquid content at different froth depths (from the bottom to the top) b) 13 mm, c) 33 mm, d) 53 mm at various flotation times
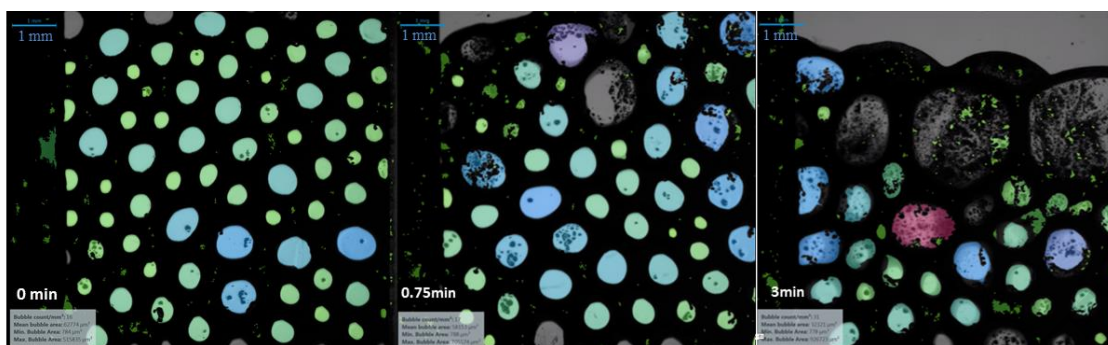
Figure 6 - Recorded images of the froth structure at different flotation times at camera height of 60 mm, i.e. froth height from 9.25 mm to 16.75 mm
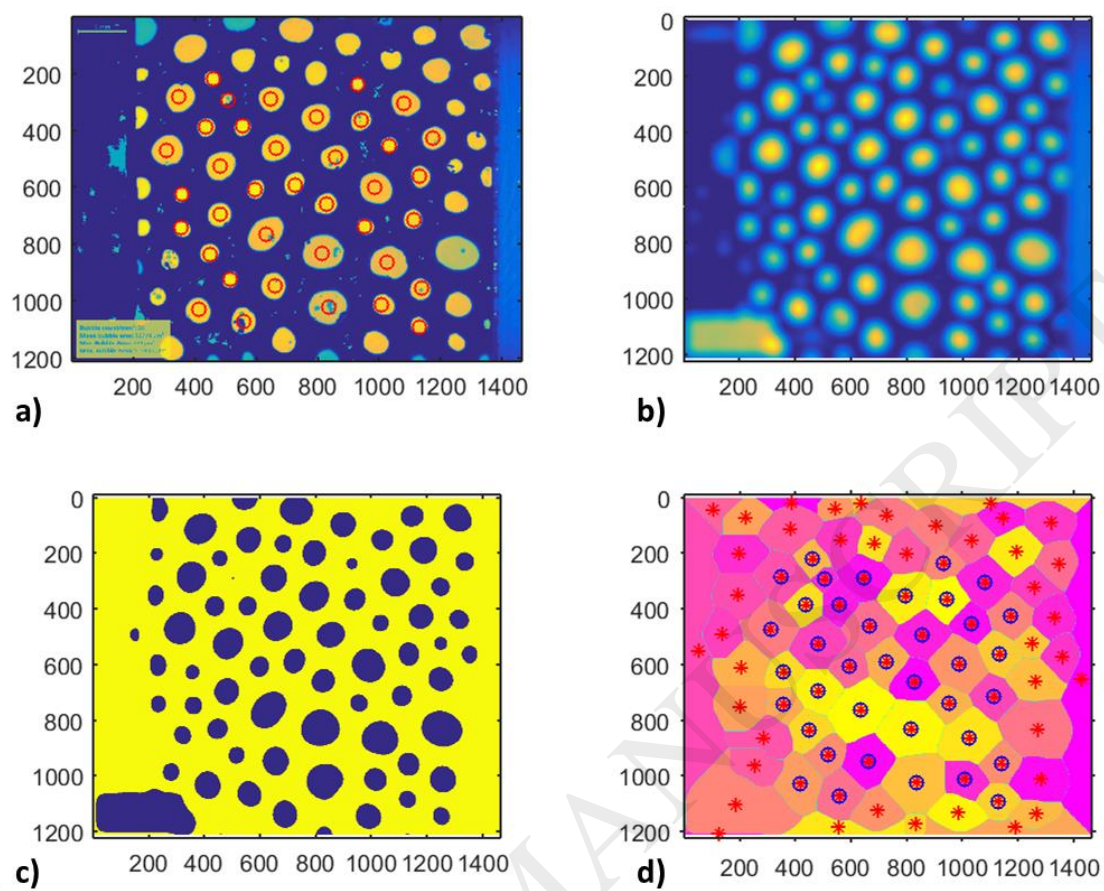
Figure 7 – Bubble size evaluation with original frame obtained from DFA 100 a) filtered image b) binarized image c) and the cell skeleton image d) analyzed bubbles are marked with a circle.

24
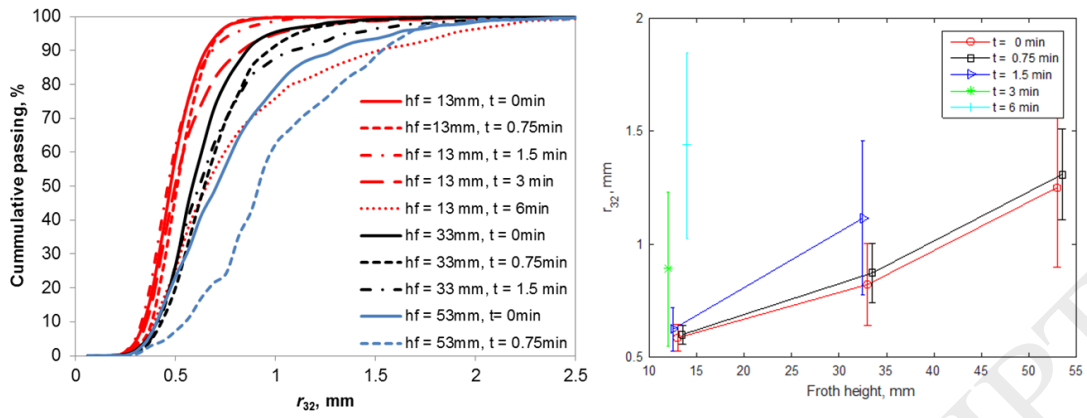
Figure 8 – Distribution of equivalent radius of bubble size (left) and Sauter mean radius (right) as a function of flotation time and froth height (the froth heights were calculated from the position of the camera and liquid level). Error bars represent one standard deviation of r_{32}
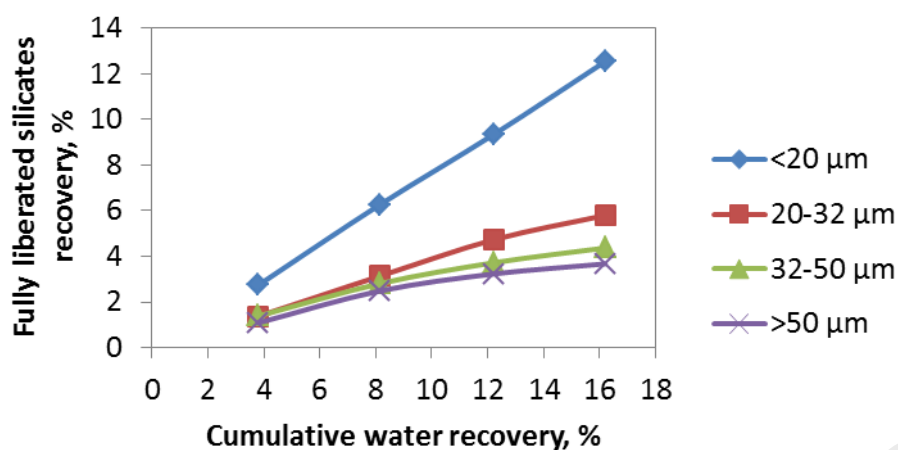
25

Figure 9 - Correlation between the fully liberated silicate particle recovery in different particle size fractions against the water recovery
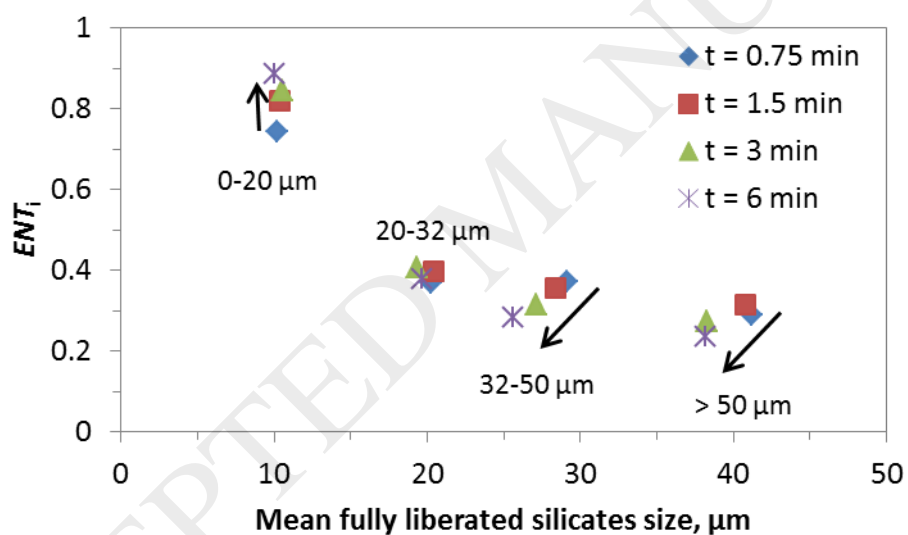

Figure 10 - The degree of entrainment for different size fractions of fully liberated silicate particles extracted from MLA plotted against the mean size for different flotation times
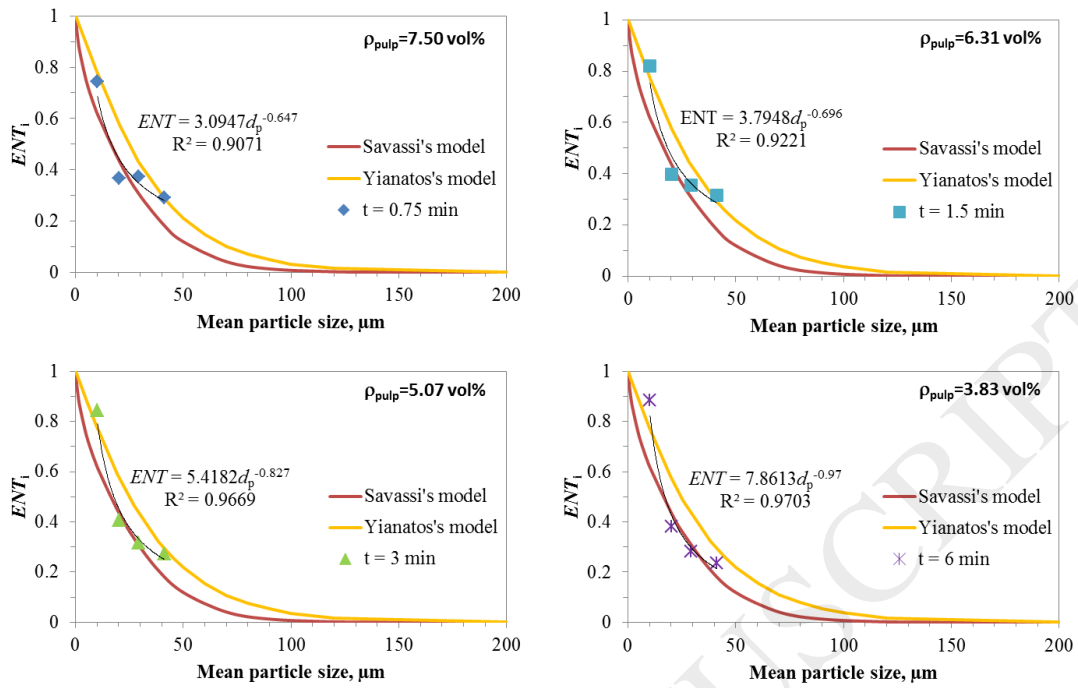
Figure 11 - The fitting curves using Savassi and Yianatos models to the experimental data for different flotation times (Savassi model: V_g = 2 l/min, A_{cell}= 12,750 mm², h_F=0.5 cm, ξ = 39.14 μm, and Yianatos model: $d_{p,0.5}$ = 24.71 μm)
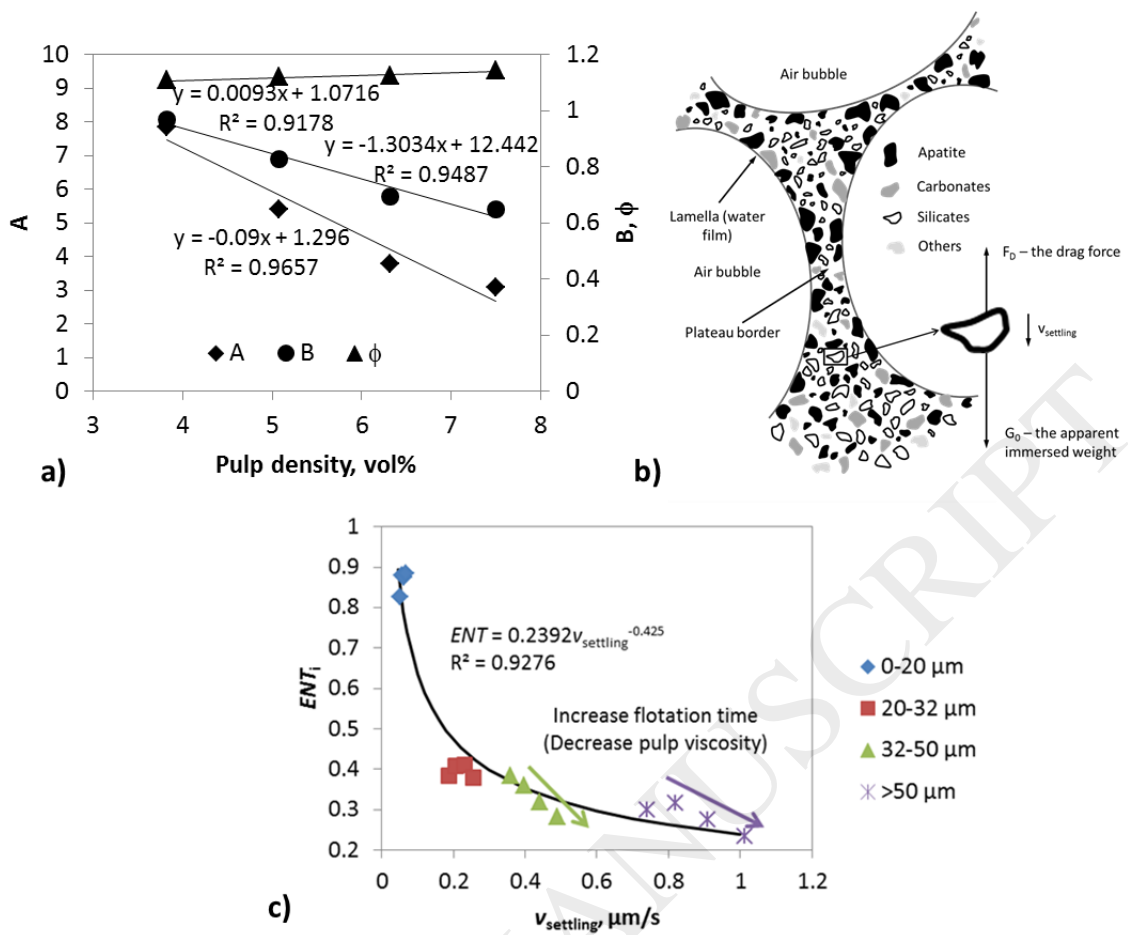
Figure 12 a) The format of the equation of fitting curves appear and drainage parameters as a function of pulp density; b) Schematic of a plateau border and its associated lamella (after Ross and Van Deventer (1988)) and forces acting on a particle at the pulp/froth interface; c) The degree of entrainment at different flotation times as a function of $v_{settling}$